# Generation and Characterization of Compositional Gradient Structure in the Biodegradable Chitosan/Poly(ethylene oxide) Blend

**Nobuyuki Osugi, Tungalag Dong, Bayar Hexig, Yoshio Inoue**

*Department of Biomolecular Engineering, Tokyo Institute of Technology, Nagatsuta 4259-B-55, Midori-ku, Yokohama 226-8501, Japan*

Received 19 September 2006; accepted 27 November 2006
DOI 10.1002/app.25996
Published online 28 February 2007 in Wiley InterScience (www.interscience.wiley.com).

**ABSTRACT:** Bio-inspired gradient materials based on the biodegradable polymer blend are expected to be indispensable to the new approaches for biomedical applications. In this study, multi-step casting self-organization on the aluminum surface are used to control the compositional distribution in the blend films of biodegradable chitosan and poly(ethylene oxide). By this way, three kinds of compositional gradient, i.e., pseudobilayer (PG), gradient (G) and semigradient (SG) blend films, along the film thickness were prepared. Their compositional morphologies were evaluated by means of ATR-FTIR and FTIR mapping measurements. In addition, the moisture absorption behavior and the mechanical properties of the gradient film were characterized with referring their gradient morphologies. It is found that the compositional G films has better mechanical properties compared with those of the PG and SG films in both the dry and wet states. © 2007 Wiley Periodicals, Inc. J Appl Polym Sci 104: 2939–2946, 2007

**Key words:** gradient material; biodegradable polymer; thermal property; moisture absorption; mechanical property

## INTRODUCTION

Recently, functionally gradient materials (FGMs) have attracted much attention since the novel materials have some superior properties, which cannot be obtained from homogeneous materials.[1] In FGMs, the property gradient in the material is caused by a position-dependent chemical composition, microstructure or atomic order, which contributes to distribute thermal stresses, to reduce mechanical stress, and to improve interfacial bonding between dissimilar materials.[2] This kind of materials also provide other functional properties depending on the constituents of their composites, and can be used to prepare, e.g., gradient optical materials and multifocal lenses.[3–5]

Recently, the concept of FGMs was first and successfully implemented as a new advanced functional inorganic composite for use in the space shuttle.[6] Since then, a number of theoretical and experimental research groups have paid considerable attentions on FGMs of metallic and ceramic materials.[7–9] The concept of FGMs may be applicable to almost all the fields of materials science, including polymer composites and biomaterials. However, the efforts on functionally gradient polymeric materials[10] and preparation methods are really weak, and not enough to develop FGMs for the potential application,[11,12] such as the application in biomedical field.

Today, the development of new biomaterials for applications is one of the challenging tasks for materials science. Biological assemblies lend an insight into the design concepts of new materials.[13] When considering several kinds of the biological materials, we often observe a number of designing principles that have not been usually used in traditional materials processing. One remarkable feature of biomaterials is the formation of hierarchical structure. Graduations in composition, microstructure, and porosity are found most commonly in biological structures such as bamboo,[14] shell, teeth, and bone, where the strongest elements are located in regions that experience the highest stress.[1] Learning from nature, our research interests aim to engineer biodegradable polymeric FGMs that are more applicable and damage-resistant than their conventional homogeneous materials.[15]

Chitosan [β-(1,4)-2-amino-2-deoxy-D-glucopyranose polymer] is a natural polysaccharide derived by deacetylation of chitin, which is the second most abundant biopolymer in nature after cellulose.[16] The production of chitosan from crustacean shells, wastes of the seafood industry, is economically feasible.[17] Compared with other polysaccharides, chitosan has several important advantages, including biocompatibility, biodegradability, and nontoxicity. Chitosan can be used as artificial skin to accelerate

*Correspondence to:* Y. Inoue (inoue.y.af@m.titech.ac.jp).

Journal of Applied Polymer Science, Vol. 104, 2939–2946 (2007)

ulcer healing of wound or a biocompatible vehicle for the sustained release of drug.[18] Chitosan's positive surface charge and biocompatibility enable it to effectively support the cell growth.[19] However, some intrinsic drawbacks of chitosan, make it not very appropriate for some biomedical applications.

Poly(ethylene oxide) (PEO), a semicrystalline polymer, has attracted much attention, and its properties has been extensively investigated both experimentally and theoretically during recent decades.[20] PEO is a biocompatible, biodegradable, and water-soluble polymer.[21] These specific features make it applicable for drug delivery purposes, and also it has potential for other biomedical applications in the future.

The aims of this research are to generate compositional gradient structure in the chitosan/PEO blend under water solvent and to establish a technique to generate a variety of compositional gradient structures. Since, chitosan is superior in biocompatibility and bioactivity and PEO has a property to be adhesive, the compositional gradient chitosan/PEO film was expected to be a material having the properties of both polymers. Moreover, it is desirable to use rather than aqueous solvent not organic solvent for generation of gradient materials from the viewpoint of environment and toxicity. In this study, three kinds of compositional gradient films with different gradient profile were prepared, and their thermal properties, moisture absorption, and the mechanical properties were characterized.

## EXPERIMENTAL SECTION

### Materials

Chitosan sample, supplied by Unitika, Kyoto, Japan, was used without further purification. The degree of deacetylation (GluN%) was determined by colloidal titration and Fourier transformed infrared (FTIR) spectroscopy to be 70 and 61%, respectively. However, we could not estimate the molecular weight and polydispersity of chitosan sample, as high-molecular weight chitosan sample is insoluble in any available solvent for GPC measurement. PEO ($M_v$ = 3,00,000) was purchased from Aldrich Chemical, Tokyo, Japan.

### Sample preparation

Chitosan (2 wt %) solution was prepared by dissolving chitosan in the 1 wt % acetic acid solution and stirring for 48 h at ambient temperature. PEO (2 wt %) solution was prepared by dissolving PEO in distilled water with stirring for 48 h at 70°C. Then, the two kinds of solutions were mixed and were further stirred for 24 h, the final chitosan/PEO blend ratios in the dry state were 80/20, 60/40, 50/50, 40/60, 20/80 (wt/wt).

1. Pseudobilayer gradient (PG) film: The PG film was prepared at 50°C by a multi-step casting method as described below. About 1 mL of chitosan solution was repeatedly poured at a time onto the aluminum dish, at intervals of 20 min, until the total volume of the poured chitosan solution became 8 mL. The interval of 20 min ensured that more than half of the volume of solvent had evaporated. Then, about 2 mL of chitosan/PEO (50/50; wt/wt) blend solution was poured on the chitosan layer. After 40 min, about 1 mL of PEO solution was poured on it, again at intervals of 20 min eight times.
2. Gradient (G) film: The G film was prepared by the same method as (1). First, about 1 mL of chitosan solution was repeatedly poured onto the aluminum dish at intervals of 20 min until the total volume of the poured solution became 3 mL. Then, about 1 mL of chitosan/PEO (80/20; wt/wt) blend solution was poured onto the chitosan layer at intervals of 20 min until the total volume of the poured solution became 3 mL. Another blend solutions (chitosan/PEO; 60/40, 50/50, 40/60, 20/80; wt/wt) with increasing PEO content were also poured sequentially and similarly as mentioned above.
3. Semigradient (SG) film: The SG film was manufactured using self-organization method.[22] The mixture with the same weight percentage of chitosan and PEO was stirred by 24 h and then cast on an aluminum dish at 50°C.

Based on the above methods, the three kinds of gradient film with different gradient extent were obtained. All of the prepared films were stored for more than 2 weeks at 50°C to eliminate the solvent and ensure the complete crystallization of the components in the films.

### ATR-FTIR measurement

The attenuated total reflectance fourier transformed infrared (ATR-FTIR) spectra were recorded on the AIM-8800 FTIR spectrometer (Shimazu, Japan) to analyze the chemical composition of the film surfaces. The spectra were recorded with the sum of 64 scans at a resolution of 4 $cm^{-1}$.

### FTIR mapping measurement

The sample for FTIR mapping measurement was sliced from along the thickness direction the film by the microtome. FTIR mapping measurements were carried out on the same AIM-8800 FTIR microscope equipped with Diamond EX′ Press. A square aperture of 30 × 30 μm$^2$, which can automatically more under a setting program, was set on one side of the cross section. The square aperture was displaced about 10 times by a step of 20 μm. The sum of 64 scans with a resolution of 4 cm$^{-1}$ was averaged at each step. The spectra were accumulated together to make a mapping mode spectrum.

### Water-uptake

The water-uptake measurement was carried out with following the method of Anglés and Dufresne.[23] The chitosan is known to be sensitive to liquid water and can partially dissolve after long time exposure to water. First, sheets with 20 × 20 mm$^2$ were dried at 0% RH on the $P_2O_5$ powder for 1 week. After being weighed, they were conditioned at 20–25°C in a desiccator containing $CuSO_4 \cdot 5H_2O$ saturated solution to ensure a relative humidity of 98%. The weight of all sample were monitored by weighing until a constant weight was reached. The water uptake was calculated as follows:

$$\text{water content}(\%) = \left(\frac{W_f - W_i}{W_f}\right) \times 100$$

where $W_f$ and $W_i$ are the weights of the sample after $t$ time conditioning at 98% RH and the initial weight of the sample at 0% RH, respectively.

### Differential scanning calorimetry

Differential scanning calorimetry (DSC) thermograms were recorded on a Seiko DSC-220U instrument with a SSC-5300 control system (Seiko Instruments, Tokyo, Japan). Each sample, sealed in an aluminum pan, was heated from − 40 to 150°C at a rate of 10°C min$^{-1}$. The melting temperature ($T_m$) and melting enthalpy ($\Delta H$) of PEO were determined from the first heating scan.

### Tensile test

The tensile testing of the sample was performed on a EZ testing machine (Shimadzu, Tokyo, Japan). The gauge length and crosshead speed are 22.25 mm and 2 mm/min, respectively. The films were cut into the standard tensile samples by a dumbbell-shaped knife. Each type of film were tested at least five times of at (22 ± 3)°C and a relative humidity of (25 ± 5)%.

## RESULTS AND DISCUSSION

### Gradient structure

Scheme 1 shows the schematic illustration of a true bilayer (a), homogenous (b), and gradient structures (c–e). In the gradient composite materials, the composition of both the components change continuously along the film thickness direction from the surface of one material to that of the other material. Scheme 1(c) shows a PG structure, exhibiting a narrower compositional gradient only in the middle region of the film. Scheme 1(d) shows a well-structured compositional gradient structure (G). Scheme 1(e) shows a semigradient structure (SG), here a comparatively small fraction of two components each other diffused from the one side to the another side.

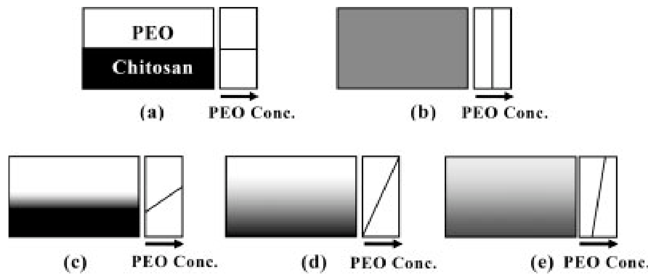


**Scheme 1** Schematic diagram of (a) bilayer, (b) homogenous, (c) pseudobilayer gradient (PG), (d) gradient (G), and (e) semigradient (SG) structure.

### Characterization of compositional gradient structure

FTIR spectroscopy was used to directly characterize the spatial compositional variation in the sample. ATR-FTIR can give information about the chemical composition in the range from the top surface into the depth of a few micrometers. Figure 1 shows the ATR-FTIR spectra of chitosan and PEO in their pure states. The characteristic IR absorption peaks peculiar to chitosan were observed at ∼ 1650 and 1550 cm$^{-1}$, which correspond to the amide band I and II, respectively.[24,25] The characteristic peak at ∼ 844 cm$^{-1}$, corresponding to the C—O stretching, was observed for PEO. These characteristic peaks were used to monitor the compositional change of chitosan and PEO along the thickness direction of the blend films.

At first, the chemical composition of both the surfaces of the resulted compositional gradient films was examined by ATR-FTIR measurements, as shown in Figure 2. Figure 2(a) shows the spectra of the two side surfaces of PG film. Only the IR-spectra corresponding to those of neat chitosan and PEO were observed for the aluminum side and air side surface, respectively. The same result was observed for the G film, as shown in Figure 2(b). In Figure 2(c), both the spectra of the aluminum side and the air side surfaces consists of those of chitosan and PEO, indicating the presence of both the components on the surface area of both sides of the SG film. However, in this case, the aluminum side is rich in chitosan, whereas the air side is rich in PEO,

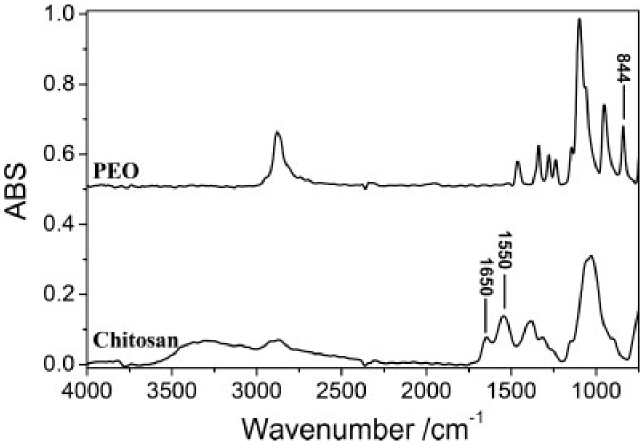


**Figure 1** ATR-FTIR spectra of pure chitosan and pure PEO films.

which were confined by comparing the relative intensities of their characteristic peaks.

Second, the compositional gradient structure along the film thickness direction was monitored by FTIR mapping measurement. A slice that is thin enough to follow the Lambert-Beer law was prepared by microtome slicing. The results of FTIR mapping measurements on the cross section of the slices are shown in Figure 3. The intensities of the peaks at 1650 and 1560 cm$^{-1}$ corresponding to the amide band I and II of chitosan increase along the film thickness direction from the air side to the aluminum side, whereas that of the PEO C-O stretching band at 844 cm$^{-1}$ decreases along the same direction.

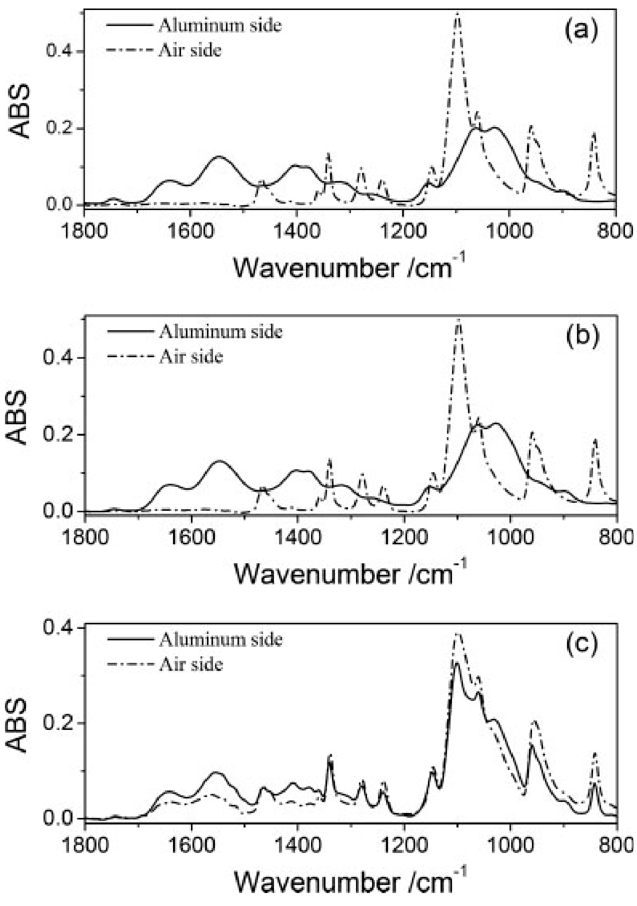


**Figure 2** ATR-FTIR spectra of the aluminum side and the air side of (a) PG, (b) G, and (c) SG films.

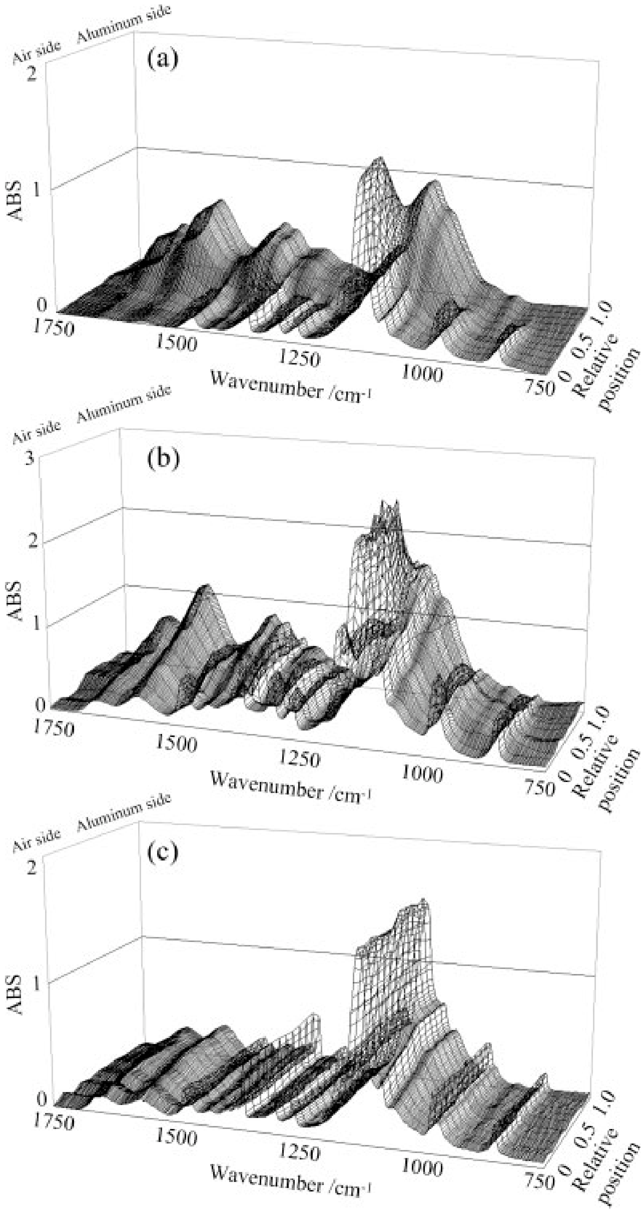


**Figure 3** Results of FTIR mapping measurements on the cross section along the direction vertical to the film surface for (a) PG, (b) G, and (c) SG films.

Although, three films show similar overall trends in compositional gradient, there was distinct difference in the extent of the gradient. Figure 4 illustrates the change of the intensities of the chitosan amide bands and the PEO C—O band along the thickness direction. Figure 4(a) shows that the gradient film of the PG type, in which the compositions of both

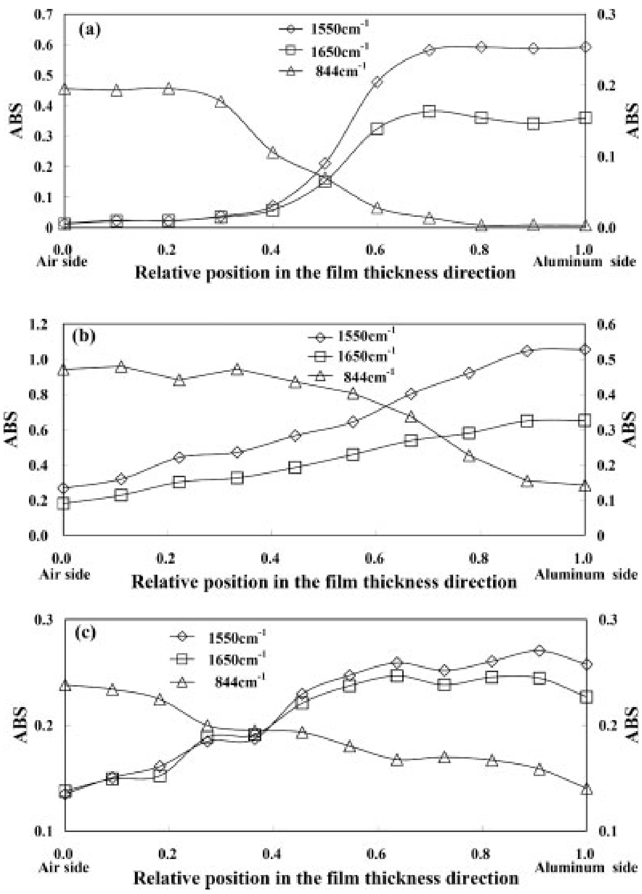


**Figure 4** Plot of the peak intensity of the amide band I and II absorption centered at 1650 and 1550 $cm^{-1}$, and that of the PEO C—O stretching absorption at 844 $cm^{-1}$ along the film thickness direction, respectively.

components were replaced in a narrow range, was formed along the film thickness direction. Figure 4(b) shows that the G type film is well-structured continuous compositional gradient along the film thickness direction. However, only a little compositional gradient structure is generated in the SG film, which is close to that in the homogenous blend film, as shown in Figure 4(c).

### Miscibility between chitosan and PEO

At present, several functionally gradient polymeric materials are efficiently created based on the miscible polymer blend systems.[26–28] Mutual diffusion of the miscible polymer components in the interfacial region of the melt-state bilayer of two component polymers is necessary for a generation of gradient concentration. Therefore, the miscibility between chitosan and PEO might be one of important factors for the generation of compositional gradient structure in the chitosan/PEO blend.

FTIR measurements gave many information about the miscibility of chitosan and PEO. Figure 5 shows ATR-FTIR analyses of chitosan, PEO, and their SG film (air side). The pure chitosan shows the amide band I and II in the region of 1500–1700 $cm^{-1}$ [Fig. 5(a)]. The O—H and N—H stretching vibrations of chitosan can be characterized by the broad peak in the region of 3000–3600 $cm^{-1}$ [Fig. 5(b)]. As PEO shows no absorption in these regions, any changes observed in these regions should be directly attributed to those in the amide or hydroxyl group environment of chitosan, such as hydrogen-bond formation and morphology change.

As shown in Figure 5(a), the amide band II of chitosan is observed at 1550 $cm^{-1}$. Upon blending with PEO, a second band appears at a higher wavenumber (1562 $cm^{-1}$) beside the band centered at about 1550 $cm^{-1}$ for the SG film. The second band should be attributed to the associated amide vibration, and confirm the formation of interassociated hydrogen bonds between chitosan and PEO. The O—H and N—H stretching bands of chitosan, PEO and their blend system, also suggest a formation of intermolecular interaction between chitosan and PEO, as shown in Figure 5(b). The main band of chitosan, centering at 3282 $cm^{-1}$, is attributed to the self-associated O—H or N—H group because of its appearance at a low wavenumber. By blending chitosan and PEO, a new band centering at about 3355 $cm^{-1}$ appears, which should be induced by the formation of the intermolecular hydrogen bonds. Although, no significant changes of ATR-FTIR spectra in the range from 750 to 4000 $cm^{-1}$ were observed for the PEO in the SG film, some disappearance of crystallinity of PEO in the G and dry SG film was observed by DSC analyses, as shown in Table I. It is suggested that the chitosan/PEO blends are partially miscible, which is in agreement with literature.[24,25] These hydrogen-bonding interactions between both the components should improve their miscibility and

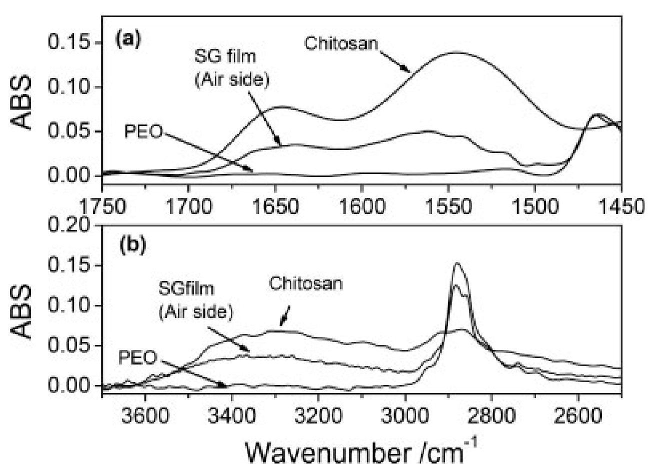


**Figure 5** ATR-FTIR spectra of chitosan, PEO, and their SG film (air side).

**TABLE I**
**Melting Point $T_m$ and Heat of Fusion $\Delta H$ of PEO Component in Chitosan/PEO Gradient Films**

| Sample | Thermal properties | Storage time (h) 0 | 2 | 6 | 12 | 25 | 50 | 100 |
|---|---|---|---|---|---|---|---|---|
| PG film | $T_m$/°C | 66 | 55 | 44 | 38 | N.D. | N.D. | N.D. |
| G film | $T_m$/°C | 65 | 53 | 53 | 47 | N.D. | N.D. | N.D. |
| SG film | $T_m$/°C | 65 | 50 | 46 | 45 | N.D. | N.D. | N.D. |
| PEO | $T_m$/°C | 66 | 66 | 62 | 53 | 41 | N.D. | N.D. |
| PG film | $\Delta H$/J/g | 142 | 89 | 45 | 10 | N.D. | N.D. | N.D. |
| G film | $\Delta H$/J/g | 122 | 75 | 76 | 38 | N.D. | N.D. | N.D. |
| SG film | $\Delta H$/J/g | 114 | 104 | 84 | 64 | N.D. | N.D. | N.D. |
| PEO | $\Delta H$/J/g | 150 | 144 | 144 | 113 | 26 | N.D. | N.D. |

N.D., Could not be detected.

decrease the degree of phase separation during the generation of gradient structure.

## Water-uptake

Figure 6 shows the change of water uptake versus storage time during the conditioning at 98% RH. We can differentiate two zones in each curve, suggesting the presence of the kinetically different water absorption processes. For a pure chitosan film, at storage time shorter than 50 h (Zone I) the water absorption is rapid, whereas after 50 h storage time, it becomes slow and reaches a plateau (Zone II). The water absorption by PEO is very slow, with increasing the storage time to 100 h, the water content in the PEO film is close to that in the chitosan film. For the three kinds of gradient films, the water absorptions at the equilibrium were obtained from Figure 6 by taking a value at the Zone II, where the water content increases a little against the storage time. All three films show almost the same values of water absorption in the equilibrium state. However, the water absorption rate appears different among the three

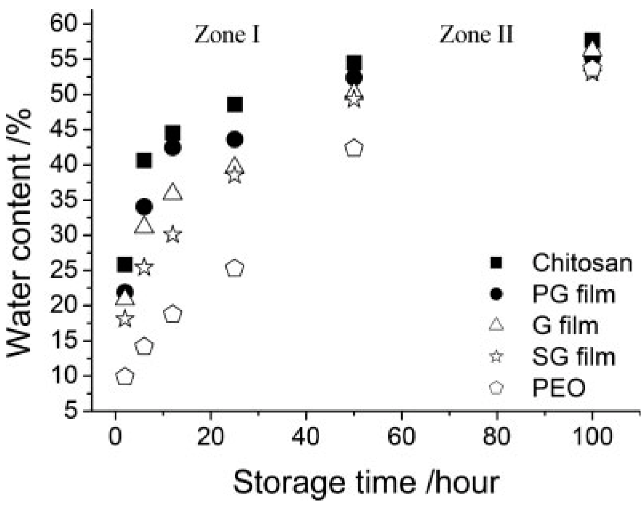


**Figure 6** Plot of the water content versus storage time.

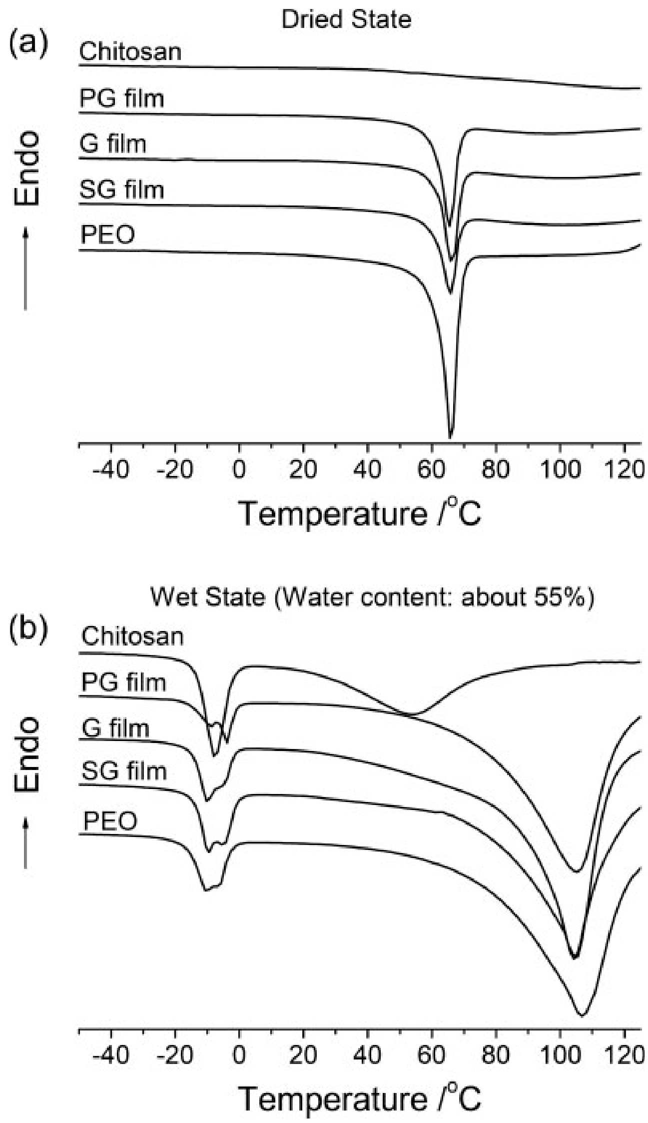


**Figure 7** DSC thermograms of pure chitosan, PG film, G film, SG film, and PEO with (a) dry and (b) wet states (water content: about 55%).

kinds of gradient films in the Zone I. In this region, the water absorption rate increases in the order of SG < G < PG film. It seems that the fast water absorption is due to the presence of chitosan rich phase.

## Thermal properties

As typical examples, Figure 7(a,b) show the DSC first scans for chitosan, PEO and their gradient films with dry state and wet state after moistened for 100 h, respectively. The dry chitosan did not show distinct melting peak in the heating scans, whereas the dry PEO showed the melting peak at 66°C. However, the melting peak of PEO was disappeared after moistened for 100 h, indicating that PEO became amorphous. As shown in Figure 7(b), the two exothermal peaks were detected at about 0 and 100°C for each DSC curve, corresponding to the fusion and the evaporation of water, respectively.

Since chitosan does not show any distinct melting transition detectable by DSC, only the thermal properties of PEO are available by DSC measurement. The values of the melting temperature ($T_m$) and melting enthalpy ($\Delta H$) of PEO and the chitosan/PEO gradient films with various storage times were summarized in Table I. For the dry state, the $\Delta H$ value of the PG film is close to that of pure PEO. However, the $\Delta H$ values of the G and the SG film are lower than that of the pure PEO. This may be due to the formation of the hydrogen bond between both the components, resulted in the PEO component being well dispersed.

For their wet state, the $T_m$ and $\Delta H$ values of PEO in the pure and blend state are decreased with the increase of storage time. When the storage time exceeded 25 h for three gradient films, the $\Delta H$ values became zero, indicating that the crystalline phase of PEO changed into the amorphous state. It is also seen that the rate of losing crystalline phase in the PG film is the fastest. In fact, since the water-uptake rate of this film is very quick, larger amounts of water were incorporated into the matrix with longer storage time.

### Tensile test

Biological materials are usually composed of soft and wet materials in the body, and are capable to undergo large deformation.[29] A variety of kinds of the interactions that biological materials experience occur through the mechanical contact.[30] Therefore, to develop bio-inspired materials, it is necessary to quantify the mechanical properties. Here, we performed the tensile test for chitosan, PEO and their gradient films with 0 and 20 wt % moisture content. The tensile stress and strain of different samples are compared in Figure 8. In the dry state, as shown in Figure 8(a), the chitosan film is very brittle, exhibiting a low break strain and very high stress at break. The PEO film shows the low break strain and low stress at break. The strain and the stress of the SG film are greatly decreased, since the PEO is almost dispersed in the full region that acts as diluent for chitosan. Both the PG and the G films show the elongation-at-break value nearly 12%, but the G film exhibits a lower elastic modulus and break stress.

Here, all samples were tested in a wet state at 25°C. These results showed a significant difference in the stress-strain behavior relative to those for the dry samples and the break stresses were lower by 50% from those of the dry samples. However, the samples endured a longer break strain. This phenomenon should be attributed to the existence of water molecules, which can be regarded as plasticizers to the hydrophilic matrix. They can combine the chitosan and PEO molecules through the hydrogen bonding interaction, and also swell the matrix. Consequently, the mobility of these matrix molecules is largely enhanced, leading in turn the increase of the chain flexibility. It is noteworthy that the G film not only preferably kept the strain break but also greatly decreased the elastic modulus and stress at break, exhibiting properties as a flexible material.

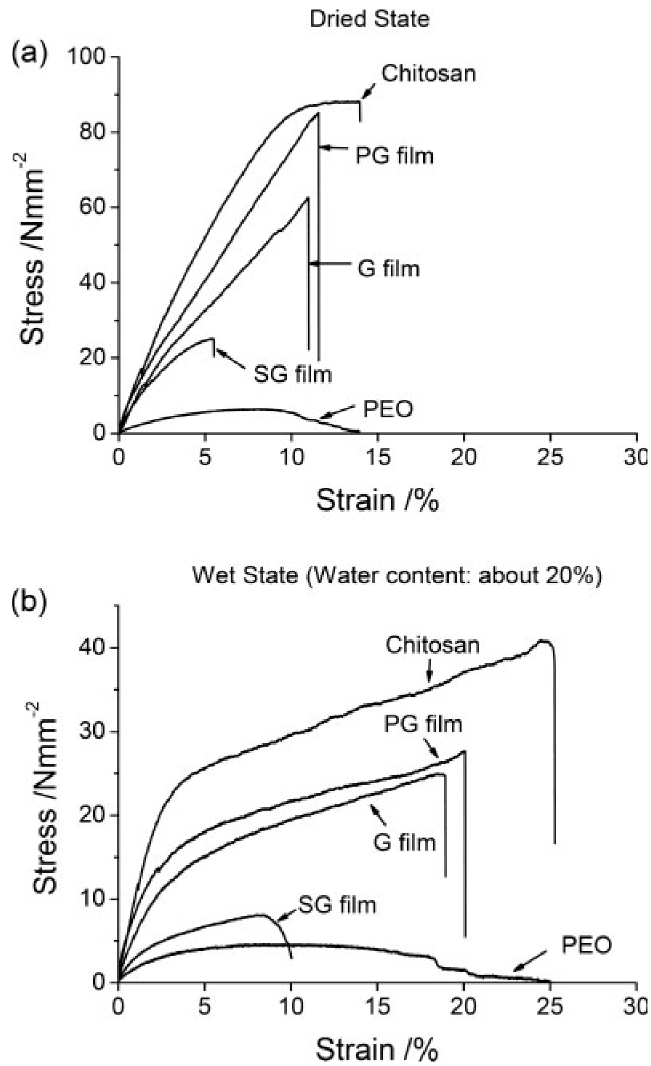


**Figure 8** Stress-strain curves of the samples with water content 0 (a) and 20 wt % (b).

## CONCLUSIONS

The biodegradable chitosan/PEO blend films with different extent of compositional gradient were prepared by multi-step casting and self-organization methods. In the three kinds of gradient films, the G film has a nearly ideal compositional gradient structure, i.e., the composition in this film changes gradually from 100% chitosan (0% PEO) at the one surface to 0% chitosan (100% PEO) at the another surface, as characterized by FTIR microscopy and ATR-FTIR analyses. Both FTIR and DSC analysis suggested that the chitosan/PEO blends are partially miscible, which can weaken their phase separation during the generation of gradient structure. In addition, we performed the tensile testing for the compositional gradient films, and those with 20% moisture content are carried out. Compared with the dry films, the most striking feature of the wet films comes from the important increase of yield strain. Especially, the G film not only preferably kept the strain break but also greatly decreased the elastic modulus and stress at break, exhibiting a properties characteristic of the flexible material, regardless of dry or wet state. This unique combination of properties should open new applications hitherto inaccessible to the other gradient films and neat polymers.

## References


1. Akiyama, S.; Kanoh, Y. Kobunsi 2000, 49, 32.
2. Suresh, S. Science 2001, 292, 2447.
3. Zuccarello, G.; Scribner, D.; Sands, R.; Buckley, L. J Adv Mater 2002, 14, 1261.
4. Kryszewski, M. Polym Adv Technol 1998, 9, 244.
5. Ma, D.; Lupton, J. M.; Beavington, R.; Burn, P. L.; Samuel, I. D. Adv Funct Mater 2002, 12, 507.
6. Quilin, F.; Xingheng, X.; Xingfang, H.; Jingku, G. Mater Sci Eng A 1999, 261, 84.
7. Uemura, S. Mater Sci Forum 2003, 1, 423.
8. Yang, X.; Masunoto, H.; Someno, Y.; Hirai, T. J Vac Sci Techol 1998, 16, 2926.
9. Moriguchi, H.; Tsuzuki, K.; Itozaki, H.; Ikegaya, A.; Hagiwara, K.; Takasaki, M.; Yanase, Y.; Fukuhara, T. SEI Tech Rev 2001, 51, 121.
10. Carl, G. S., Jr.; Eidelman, N.; Deng, Y.; N. R. Washburn. Macromol Rapid Commun 2004, 25, 2003.
11. Agari, Y.; Shimada, M.; Ueda, A. Macromol Chem Phys 1996, 19, 2017.
12. Ikejima, T.; Inoue, Y. Macromol Chem Phys 2000, 201, 1598.
13. Ryadnov, M. G.; Woolfson, D. N.; Nat Mater 2003, 2, 329.
14. Amada, S.; Untao, S. Compos B Eng 2001, 32, 451.
15. Hexig, B.; Alata, H.; Asakawa, N.; Inoue, Y.; J Polym Sci Part B: Polym Phys 2005, 43, 368.
16. Shahidi, F.; Arachchi, J. K. V.; Jeon, Y. J. Trends Food Sci Technol 1999, 10, 37.
17. Kumar, M. N. V. R.; React Funct Polym 2000, 46, 1.
18. Cho, Y. W.; Han, S.; Ko, S. W. Polymer, 2000, 41, 2033.
19. Park, K. I.; Yang, J.; Jeong, J. H.; Bom, H. S; Harada, I; Akaike, T; Kim, I. S.; Cho, S. C. Biomaterials 2003, 24, 2331.
20. Allen, C.; Maysinger, D.; Eisenberg, A. Colloids Surf B 1996, 16, 3.
21. Dormidontova, E. E. Macromolecules 2002, 35, 987.
22. Hexig, B.; Alata, H.; Inoue, Y. J Polym Sci Part B: Polym Phys 2005, 43, 3069.
23. Anglés, M. N.; Dufrense, A. Macromolecules 2000, 33, 8344.
24. Mucha, M.; Piekielna, J.; Wieczorek, A. Macromol Symp 1999, 144, 391.
25. Kolhe, P.; Kannan, R. M. Biomacromolecules 2003, 4, 173.
26. Agari, Y.; Shimada, M.; Uede, A.; Macromol Chem Phys 1996, 197, 2017.
27. Zhao, L.; Tsuchiya, K.; Inoue, Y. Macromol Biosci 2004, 4, 699.
28. Hexig, B; Alata, H; Asakawa, N; Inoue, Y. Adv Funct Mater 2005, 15, 1630.
29. Ogata, N.; Kim, W. S.; Feijen, J; Okano, T. Advanced Biomaterials in Biomedical Engineering and Drug Delivery System; Springer-Verlag: Tokyo, 1996.
30. Bruck, A. H.; Evans, J. J.; Peterson, L. M. Exp Mech 2002, 42, 361.